OPEN ACCESS
JOURNAL OF ADVANCED DIELECTRICS
Vol. 13, No. 1 (2023) 2242007 (7 pages)

DOI: 10.1142/S2010135X22420073

Dielectric temperature stability and energy storage performance of NBT-based lead-free ceramics for Y9P capacitors

Hongtian Li[*,†], Shiyu Zhou[*,‡], Jianwei Zhao[*], Tingnan Yan[*], Yuxiao Du[*], Huanfu Zhou[†], Yongping Pu[‡] and Dawei Wang[*,§,‖,**]

[*]*Shenzhen Institute of Advanced Electronic Materials, Shenzhen Institute of Advanced Technology Chinese Academy of Sciences, Shenzhen 518055, P. R. China*

[†]*Key Laboratory of Nonferrous Materials and New Processing Technology Ministry of Education, School of Materials Science and Engineering Guilin University of Technology, Guilin 541004, P. R. China*

[‡]*School of Materials Science and Engineering, Shaanxi Key Laboratory of Green Preparation and Functionalization for Inorganic Materials, Shaanxi University of Science & Technology Xi'an 710021, P. R. China*

[§]*Functional Materials and Acousto-Optic Instruments Institute School of Instrumentation Science and Engineering Harbin Institute of Technology, Harbin 150080, P. R. China*

[‖]wangdawei102@gmail.com

Received 23 September 2022; Revised 14 October 2022; Accepted 28 October 2022; Published 3 December 2022

In this work, novel $(1-x)(0.75Na_{0.5}Bi_{0.5}TiO_3)$-$0.25Sr(Zr_{0.2}Sn_{0.2}Hf_{0.2}Ti_{0.2}Nb_{0.2})O_3$-$xNaNbO_3$ (NBT-SZSHTN-xNN, x = 0.1, 0.15, 0.2, 0.25) ceramics were fabricated. The influence of co-doping of NN and high entropy perovskite oxide (SZSHTN) on the phase structure, microstructure and dielectric properties of NBT-based lead-free ceramics was investigated. Dense microstructure with a grain size of ~5 μm is observed. When x = 0.25, a wide dielectric temperature stable range of −35.4–224.3°C with a low temperature coefficient of capacitance of < 10% is achieved, fulfilling the industry standard of Y9P specification. Furthermore, excellent energy storage performance with recoverable energy density of 2.4 J/cm^3, discharge efficiency of 71%, power density of 25.495 MW/cm^3 and discharge rate < 200 ns are simultaneously obtained, which shows great potential for high temperature capacitor applications.

Keywords: NBT; lead-free; dielectric stability; capacitor.

1. Introduction

Dielectric ceramic capacitors are widely used in modern electronic devices, such as cell phones, automobiles and digital devices, because of their important functions such as pulse discharge, filtering and coupling.[1–5] The requirements of different actual environments of electronic devices ask to explore novel dielectric capacitors with high performance.[6] In order to satisfy the trend of miniaturization and integration of electronic devices, capacitors are needed to have a high dielectric constant (ε_r). In addition, operating conditions such as hybrid vehicles, electric vehicle engines and transmissions and geothermal wells require electronic components with wide interval of dielectric temperature stability.[3,7–10] According to the Electronic Industries Association (EIA) standard, the temperature coefficient of capacitance (TCC) is classified as X7R, X8R, Y9R, etc., where X and Y represent the minimum operating temperature of −50°C and −30°C, respectively, 7, 8 and 9 represent the maximum operating temperature of 125°C, 150°C and 200°C, respectively, and R represents the capacitance variation within ±15% under a given condition.[10] Therefore, it is particularly important to explore higher standard temperature stability of the dielectric.

It is well known that materials with good temperature stability are mostly derived from relaxor ferroelectrics, which exhibit broadened dielectric peaks, and the position and height of dielectric peaks can be adjusted to maintain good dielectric stability over a wide temperature range. Many studies have been conducted to modify ferroelectrics to break the long-range order and obtain relaxor ferroelectrics.[11–14] The main ferroelectrics are $BaTiO_3$ (BT), $Na_{0.5}Bi_{0.5}TiO_3$ (NBT),

**Corresponding author.

$K_{0.5}Na_{0.5}NbO_3$ (KNN), $BiFeO_3$ (BF).[2,15,16] Li *et al*. confirmed that the $BaTiO_3$–$Na_{0.5}Bi_{0.5}TiO_3$–Nb_2O_5 system doped with CoO constructed a bimodal model in a wide temperature range of −50–350°C with ε_r = 1365±15% and dielectric loss (tanδ) = 1.51%.[17] Robert *et al*. reported high ε_r of 2150±10% in the BNT-BT-*x*KNN ceramics between 43°C and 319°C.[18] High entropy perovskite oxide (HEPO) originated from the idea of high entropy alloy, which is a serial of new materials designed by solid solution of five or more elements according to the concept of "entropy engineering".[19–21] Zhou *et al*. introduced $Sr(Zr_{0.2}Sn_{0.2}Hf_{0.2}Ti_{0.2}Nb_{0.2})O_3$ (SZSHTN) into the NBT system (NBT-SZSHTN), which exhibited a good dielectric temperature stability from 52.4°C to 362°C,[15] confirming that HEPO had an effective influence for tuning dielectric properties.

Based on the above-mentioned introduction, in this work, NBT-SZSHTN ceramic was selected as the matrix due to its good dielectric properties,[15] and $NaNbO_3$ (NN) was introduced to investigate the effects on the microstructure and dielectric properties. As expected, NBT-SZSHTN-0.25NN ceramic exhibited improved dielectric temperature stability at −35.4–224.3°C along with low tanδ < 0.01 at 48.2–303.4°C. And, excellent energy storage characteristics were also obtained under an electric field of 293 kV/cm.

2. Experimental

$(1-x)(0.75Na_{0.5}Bi_{0.5}TiO_3)$-$0.25Sr(Zr_{0.2}Sn_{0.2}Hf_{0.2}Ti_{0.2}Nb_{0.2})O_3$-$xNaNbO_3$ (NBT-SZSHTN-*x*NN, *x* = 0.1, 0.15, 0.2, 0.25) ceramics were prepared by a solid-state reaction method using Na_2CO_3 (AR), Bi_2O_3 (AR), TiO_2 (CP), $SrCO_3$ (AR), ZrO_2 (AR), SnO_2 (CP), HfO_2 (CP) and Nb_2O_5 (CP) as raw materials. All chemicals were baked in a drying oven at 180°C for 24 h, and then weighed according to the stoichiometric ratio. Raw materials for NBT, SZSHTN and NN were ball milled for 24 h, respectively, and then calcined at 850°C for 3 h, 1360°C for 6 h and 850°C for 4 h at a heating rate of 5°C/min, respectively. The calcined powder was weighed according to the chemical formula and a secondary ball mill was used for 12 h. The powder was pressed into discs of 10 mm diameter and ~1 mm thickness using a cold isostatic press at a pressure of 200 MPa. Finally, the green discs were sintered in air at 1200–1250°C for 2 h.

X-ray diffraction (XRD) of sintered NBT-SZSHTN-*x*NN (*x* = 0.1, 0.15, 0.2, 0.25) ceramics was performed using a D/Max-RB diffractometer (RIGAKU). The cross-sectional morphology of the sintered ceramics after polishing and thermal etching at 1000°C for 30 min was studied and analyzed using a scanning electron microscope (SEM) equipped with an elemental analysis energy dispersive spectrometer (EDS) (Apreo 2, Thermo Fisher Scientific Waltham, MA, USA). Dielectric properties were tested by an Agilent E4980A LCR meter. The polarization-electric field (P–E) hysteresis loops were obtained by a PolyK FE analyzer. The charge/discharge properties are measured by a dielectric charge/discharge test system (CFD-003, Tongguo). The ceramic samples were coated with a high-temperature silver paste on both sides and fired at 850°C for 30 min before determining the electrical properties.

3. Results and Discussion

The XRD patterns of NBT-SZSHTN-*x*NN (*x* = 0.1, 0.15, 0.2, 0.25) ceramics are shown in Fig. 1. A secondary phase

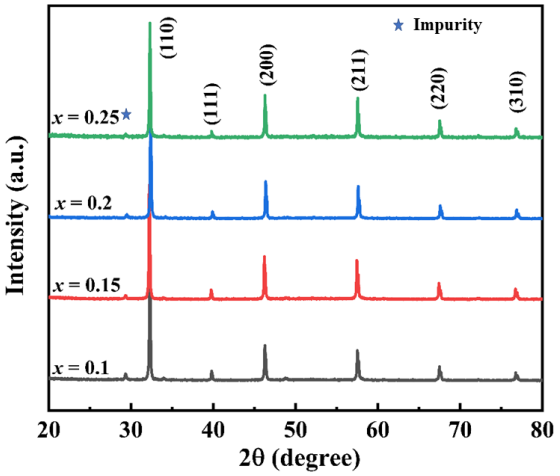

Fig. 1. XRD patterns for NBT-SZSHTN-*x*NN (*x* = 0.1, 0.15, 0.2, 0.25) ceramics.

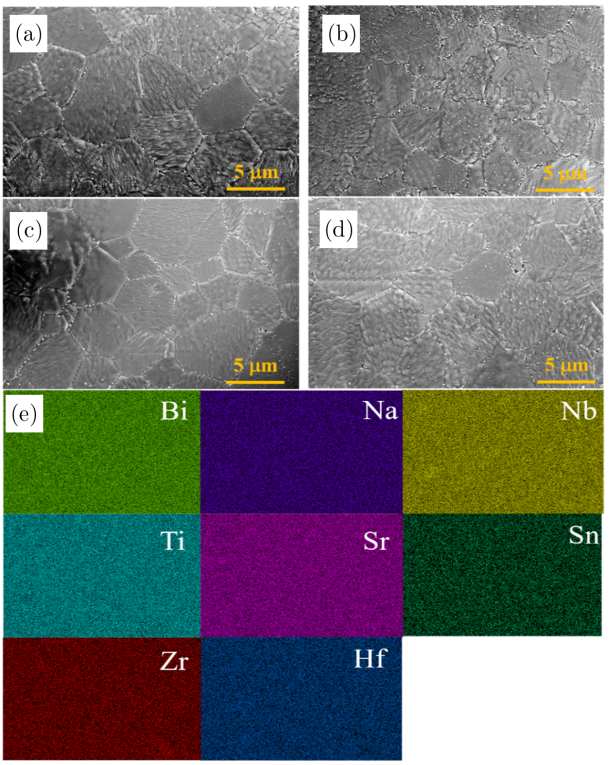

Fig. 2. SEM images of the NBT-SZSHTN-*x*NN ceramics with (a) *x* = 0.1, (b) *x* = 0.15, (c) *x* = 0.2, and (d) *x* = 0.25 and (e) EDS mapping of the NBT-SZSHTN-0.25NN ceramic.

of $Bi_2Sn_2O_7$ (PDF card No: 56-0646) is detected for all the studied compositions, which has been reported previously.[15] Furthermore, no splitting is observed in the diffraction peaks for all the studied compositions, indicating cubic phase structure by introducing both HEPO SZSHTN and NN in NBT, in agreement to the previously reported data.[15]

The SEM images of the polished and thermal-etched NBT-SZSHTN-xNN (x = 0.1, 0.15, 0.2, 0.25) ceramics are shown in Fig. 2. It can be clearly seen that all the samples exhibit a dense microscopic morphology with no obvious pores and voids, indicating high density. The grain size of ~5 μm is uniform. The EDS element mapping of NBT-SZSHTN-0.25NN is shown in Fig. 2(e), which demonstrates the uniformity of element distribution and no elemental segregation.

The temperature dependence of dielectric constant (ε_r) and loss (tanδ) of NBT-SZSHTN-xNN (x = 0.1, 0.15, 0.2, 0.25) at 1, 10, 100 and 1000 kHz are shown in Fig. 3. In the temperature range of 50°C–450°C, it can be seen that the values of ε_r remain relatively stable over a wide range (~400°C) at different frequencies, which is attributed to the broadening of two dielectric anomalies (T_s at ~100°C and T_m at ~300°C) resulted by co-doping of SZSHTN and NN. The two dielectric anomalies are related to the thermal evolution of local polar nano regions (PNRs).[15,22–25] Furthermore, as shown in Fig. 3, with the increase of NN content, both T_s and T_m are found to move to lower temperatures, and the ε_r at T_s is higher than that at T_m in all compositions. Additionally, ε_r at T_s decreases gradually with the increase of NN doping concentration, which has also been reported in KNN-doped BNT-BT systems.[26,27] For the x = 0.25 sample, a broadened dielectric plateau is formed in an ultra-wide temperature range of 100°C–300°C, which suggests that the doping of SZSHTN and NN makes ε_r of NBT insensitive to temperature, indicative of good dielectric temperature stability compared with that of other NBT-based systems. On the other hand, the tanδ of NBT-SZSHTN-0.25NN ceramics also shows good temperature stability, which is found to increase significantly only after a high temperature of 350°C. The x = 0.25 sample has a low tanδ < 0.01 in the temperature range of 48.2–303.4°C, which indicates that the doping of NN and SZSHTN reduces the temperature dependence of tanδ.

The temperature stability of capacitors is generally evaluated by the temperature coefficient of capacitance (TCC),

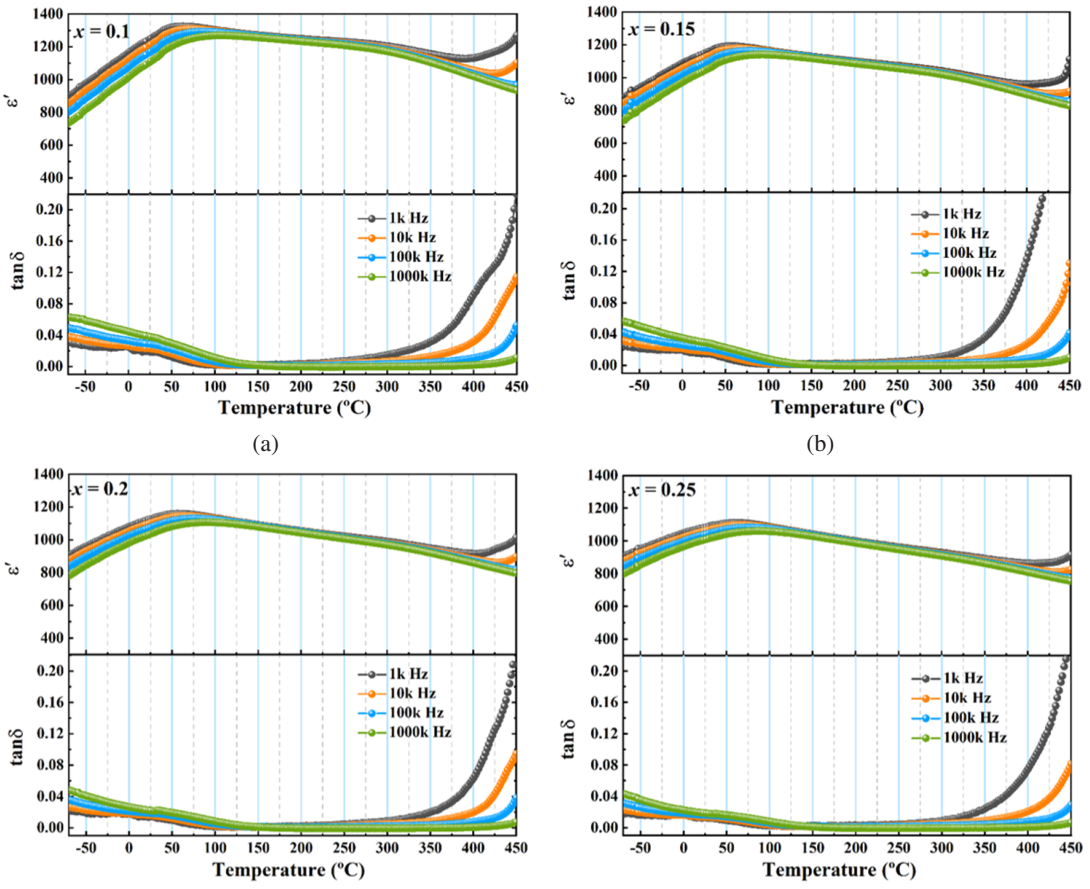

Fig. 3. Dielectric constant and loss as a function of temperature for NBT-SZSHTN-xNN ceramics (a) x = 0.1, (b) x = 0.15, (c) x = 0.2 and (d) x = 0.25.

which is described as follows:

$$\mathrm{TCC} = \frac{C_T - C_{\mathrm{base}}}{C_{\mathrm{base}}}, \quad (1)$$

where C_{base} is the capacitance at a base temperature (normally 25°C), and C_T represents the capacitance at any temperature in the operating range.[28,29] The TCC of NBT-SZSHTN-xNN (x = 0.1, 0.15, 0.2, 0.25) ceramics is calculated and plotted in Fig. 4. It is found that the TCC values of all compositions are quite low in a wide temperature range of –50–400°C. Table 1 lists the temperature ranges for all the studied compositions with TCC < 10% and tanδ < 0.01. Especially, the composition of x = 0.25 exhibits excellent dielectric temperature stability with TCC < 10% over a wide temperature range of –35.4–224.3°C, meeting the industry standard of Y9P. Consequently, the favorable dielectric temperature stability performance has been achieved at NBT-SZSHTN-0.25NN, which demonstrates that the introduction of NN and SZSHTN effectively broadens the dielectric anomalies of NBT with low TCC and wide temperature-stable range, promising for practical applications in high temperature capacitors.

The unipolar P-E loops of NBT-SZSHTN-0.25NN ceramic with different electric fields are shown in Fig. 5(a). It could be clearly seen that the overall shape of loops is slim and P_{max} gradually increases with the increase of electric field. Also, P_r changes slightly, which is beneficial to the energy

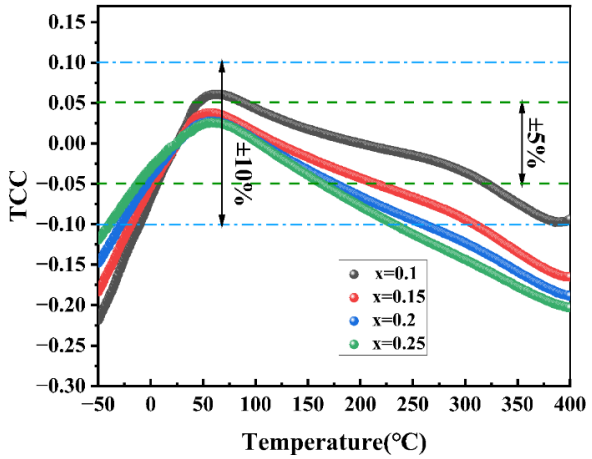

Fig. 4. The TCC of NBT-SZSHTN-xNN (x = 0.1, 0.15, 0.2, 0.25) ceramics.

Table 1. Temperature range for NBT-SZSHTN-xNN (x = 0.1, 0.15, 0.2, 0.25) ceramics with TCC < 10% and tanδ < 0.01.

Content	ε_r @ 25°C	ε_r	tanδ
x = 0.1	1249.18	–10–400°C	58–274°C
x = 0.15	1148.84	–18.9–309.9°C	49.1–295°C
x = 0.2	1128.20	–7.8–262.3°C	49.2–311.3°C
x = 0.25	1082.21	–35.4–224.3°C	48.2–303.4°C

storage performance. W_{rec} and η are calculated and plotted in Fig. 5(b). The recoverable energy density (W_{rec}) and energy storage efficiency (η) are determined by[30–32]

$$W_{\mathrm{rec}} = \int_{P_r}^{P_{\mathrm{max}}} E dp, \quad (2)$$

$$\eta = \frac{W_{\mathrm{rec}}}{W_{\mathrm{rec}} + W_{\mathrm{loss}}}. \quad (3)$$

At an electric field of 293 kV/cm, NBT-SZSHTN-0.25NN ceramic reaches a maximum value of 2.4 J/cm^3 at W_{rec} with η ~ 71%. Energy storage temperature stability is an important performance index for high temperature capacitors. Figures 5(c) and 5(d) display the variation of unipolar P-E loops and calculate W_{rec}/η for NBT-SZSHTN-0.25NN ceramics in the temperature range of 20–150°C. The W_{rec} and η values changed slightly over the temperature range of 20–150°C, with W_{rec} changing by only ±6% (–6.0 – +0.8%) and η by +5.5%, which demonstrates excellent energy storage temperature stability.

It is well known that the fast charge and discharge behavior is a key performance for ceramic capacitors. The charge/discharge characteristics of NBT-SZSHTN-0.25NN ceramics in the electric field of 40–100 kV are shown in Fig. 6. It is observed that the discharged current gradually increases with the increase of electric field in underdamped curves, with the peak current (I_{max}) of 35.7 A at an electric field of 100 kV/cm (Fig. 6(a)). The current density (C_D), power density (P_D) and discharge energy density (W_{dis}) are calculated by Eqs. (4)–(6) as follows:

$$C_D = \frac{I_{\mathrm{max}}}{S}, \quad (4)$$

$$P_D = \frac{E \times I_{\mathrm{max}}}{2S}, \quad (5)$$

$$W_{\mathrm{dis}} = \frac{R\int I^2(t)dt}{V}, \quad (6)$$

where E, S, R and V are the electric field, electrode area, load resistance, and sample volume, respectively.[21,32,33] Both C_D and P_D increase with increasing electric field, as shown in Fig. 6(b). The maximum values of C_D~509.915 A/cm^2 and P_D~25.495 MW/cm^3 are obtained at 100 kV/cm electric field, respectively. The overdamped discharge curves were tested in a closed circuit with a load resistance of 200 Ω, as shown in Fig. 6(c). The current increases as the electric field increases from 40 kV/cm to 100 kV/cm, and the I_{max} reaches ~7 A at the maximum electric field of 100 kV/cm. The W_{dis} is also found to increase with the increase of electric field, and the maximum W_{dis} of 1.93 J/cm^3 is obtained at 100 kV/cm, as shown in Fig. 6(d). All the discharge processes release 90% of W_{dis} at ~200 ns, that is the discharge time ($t_{0.9}$), indicating a fast discharge speed, which is proved to be a promising candidate for future pulse power applications.

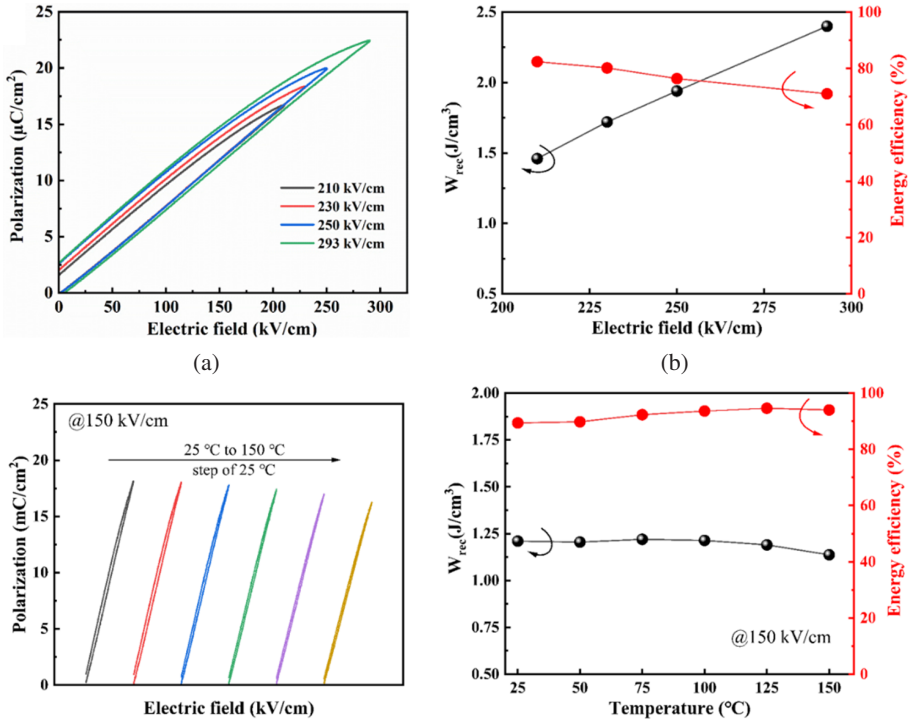

Fig. 5. Unipolar P-E loops under different electric fields for (a) NBT-SZSHTN-0.25NN (b) W_{rec} and η as a function of electric field for NBT-SZSHTN-0.25NN. (c) The temperature dependence unipolar P-E loops for NBT-SZSHTN-0.25NN at an electric field of 150 kV/cm. (d) W_{rec} and η as a function of temperature.

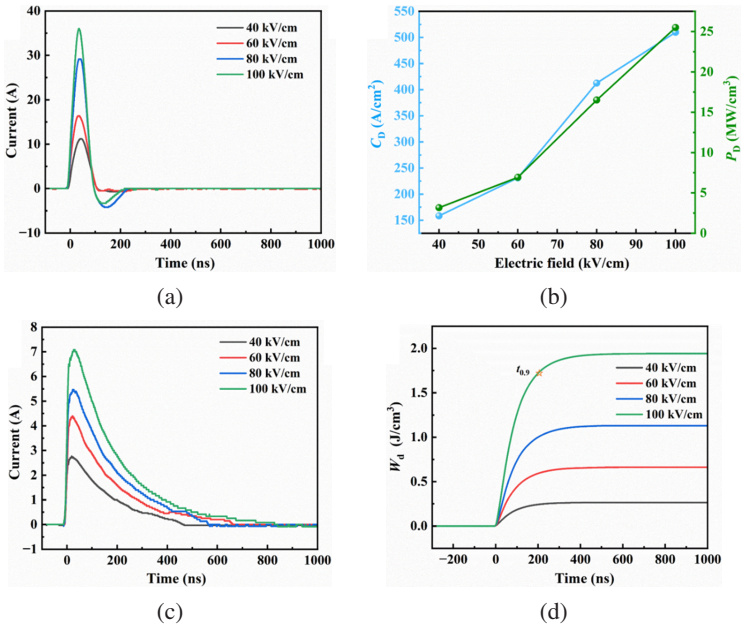

Fig. 6. Discharge behavior of NBT-SZSHTN-0.25NN ceramic (a) underdamped discharge curves, (b) current density and power density versus electric field, (c) overdamped discharge curves and (d) discharge energy density versus time.

4. Conclusion

In this work, the effects of NN and HEPO SZSHTN on the phase structure, microstructure and dielectric properties of NBT-based ceramics are investigated. XRD results showed that with the increase of NN content, the phase structure kept pseudo-cubic phase. Dense microstructure with an average grain size of ~5 μm was observed by the SEM images. With the increase of NN content, the dielectric temperature stability

was improved, which was attributed to the thermal evolution of PNRs. The optimized dielectric temperature stability has been achieved in NBT-SZSHTN-0.25NN ceramic with a low TCC < 10% in a wide temperature range of −35.4–224.3°C, satisfying the Y9P standard. Furthermore, high energy storage properties of W_{rec}~2.4 J/cm^3, η~71% and discharge behavior of C_D~509.915 A/cm^2, P_D~25.495 MW/cm^3 were also found in NBT-SZSHTN-0.25NN ceramic. Those results indicate that the introduction of both NN and HEPO SZSHTN can effectively improve the dielectric temperature stability of NBT ceramics with excellent energy storage performance, which provides a strategy for the design of novel high temperature capacitors.

Acknowledgments

This work was financed by the National Natural Science Foundation of China (51872175), the International Cooperation Projects of Shaanxi Province (2018KW-027), Guangdong Provincial Key Laboratory (2014B030301014) and the Construction of Basic Research Institutions from Shenzhen Science, Technology and Innovation Commission. H. Li and S. Zhou contributed equally to this work.

References

[1]H. Kishi, Y. Mizuno and H. Chazono, Base-metal electrode-multilayer ceramic capacitors: Past, present and future perspectives, *Jpn. J. Appl. Phys.* **42**, 1 (2003).

[2]J. Wenxu, H. Yudong, Z. Mupeng, X. Yuru, Z. Mankang, Y. Kuiyong, C. Huarong, S. Shuying and X. Jie, Advances in lead-free high-temperature dielectric materials for ceramic capacitor application, *IET Nanodielectr.* **1**, 3 (2018).

[3]R. W. Johnson, J. L. Evans, P. Jacobsen, J. R. R. Thompson and M. Christopher, The changing automotive environment: High-temperature electronics, *IEEE Trans. Electron. Packag. Manuf.* **27**, 164 (2004).

[4]M. Shiga, M. Hagiwara and S. Fujihara, $(Bi_{1/2}K_{1/2})TiO_3$-$SrTiO_3$ solid-solution ceramics for high-temperature capacitor applications, *Ceram Int.* **46**, 10242 (2020).

[5]P. R. H. Zhao, Q. Hua, L. Liu, X. Wang, Y. Wan, F. Yan, G. Zhao and D. Wang, Temperature stable (1-x)($0.9Na_{0.5}Bi_{0.5}TiO_3$-0.1Bi-AlO_3)-x$NaTaO_3$ ceramics and capacitors with ultra-wide operational range, *J. Alloys Compd.* **886**, 161315 (2021).

[6]Y. Sun, H. Liu, H. Hao, L. Zhang and S. Zhang, The role of Co in the $BaTiO_3$–$Na_{0.5}Bi_{0.5}TiO_3$ based X9R ceramics, *Ceram Int.* **41**, 931 (2015).

[7]R. S. Demcko, Evolution of high-temperature capacitors, *Proc. IEEE Electron. Components Conf.* Los Angeles, CA, 9–11 May 1988, p. 390

[8]R. Muhammad, A. Ali, J. Camargo, M. S. Castro, W. Lei, K. X. Song and D. W. Wang, Enhanced thermal stability in dielectric properties of $NaNbO_3$-modified $BaTiO_3$-$BiMg_{1/2}Ti_{1/2}O_3$ ceramics for X9R-MLCC applications, *Crystals* **12**, 10 (2022).

[9]H. L. Cheng, H. L. Du, W. C. Zhou, D. M. Zhu, F. Luo and B. X. Xu, $Bi(Zn_{2/3}Nb_{1/3})O_3$-$(K_{0.5}Na_{0.5})NbO_3$ High-temperature lead-free ferroelectric ceramics with low capacitance variation in a broad temperature usage range, *J. Am. Ceram. Soc.* **96**, 833 (2013).

[10]K. Hui, L. Chen, Z. Cen, P. Zhao, Y. Yu, L. Guo, X. H. Wang and L. T. Li, KNN based high dielectric constant X9R ceramics with fine grain structure and energy storage ability, *J. Am. Ceram. Soc.* **104**, 5815 (2021).

[11]E. A. Patterson and D. P. Cann, Relaxor to ferroelectric transitions in $(Bi_{1/2}Na_{1/2})TiO_3$-$Bi(Zn_{1/2}Ti_{1/2})O_3$ solid solutions, *J. Am. Ceram. Soc.* **95**, 3509 (2012).

[12]A. Zeb and S. J. Milne, Stability of high-temperature dielectric properties for (1-x)$Ba_{0.8}Ca_{0.2}TiO_3$-x$BiMg_{0.5}Ti_{0.5})O_3$ ceramics, *J. Am. Ceram. Soc.* **96**, 2887 (2013).

[13] D. Han, C. Wang, D. Lu, F. Hussain, D. Wang and F. Meng, A temperature stable $(Ba_{1-x}Ce_x)(Ti_{1-x/2}Mg_{x/2})O_3$ lead-free ceramic for X4D capacitors, *J. Alloys Compd.* **821**, 153480 (2020).

[14]Z. Li, C. Wang, Z. Wang, D. Zhang, Y. Qin, Q. Yang, Z. Wang, P. Zhao, S. Ma, M. Li, T. Ai, X. Yan, Y. Niu, B. Peng, S. Sun and D. Wang, Core-shell structure and dielectric properties of $Ba_{0.6}Sr_{0.4}$-TiO_3@Fe_2O_3 ceramics prepared by co-precipitation method, *Crystals* **11**, 623 (2021).

[15]S. Zhou, Y. Pu, X. Zhao, T. Ouyang, J. Ji, Q. Zhang, C. Zhang, S. Sun, R. Sun, J. Li and D. Wang, Dielectric temperature stability and energy storage performance of NBT-based ceramics by introducing high-entropy oxide, *J. Am. Ceram. Soc.* **105**, 4796 (2022).

[16]H. Ji, D. Wang, W. Bao, Z. Lu and I. M. Reaney, Ultrahigh energy density in short-range tilted NBT-based lead-free multilayer ceramic capacitors by nanodomain percolation, *Energy Stor. Mater.* **38**, 113 (2021).

[17]L. Li and B. Zhang, The effect of bimodal model on the ultra-broad temperature stable $BaTiO_3$–$Na_{0.5}Bi_{0.5}TiO_3$–Nb_2O_5 system, *Scr. Mater.* **114**, 170 (2016).

[18]R. Dittmer, W. Jo, D. Damjanovic and J. Rodel, Lead-free high-temperature dielectrics with wide operational range, *J Appl. Phys.* **109**, 346 (2011).

[19]D. B.Miracle and O. N. Senkov, A critical review of high entropy alloys and related concepts, *Acta Mater.* **122**, 448 (2017).

[20]A. Amiri and R. Shahbazian-Yassar, Recent progress of high-entropy materials for energy storage and conversion, *J. Mater. Chem. A* **9**, 782 (2021).

[21]S. Zhou, Y. Pu, X. Zhang, Y. Shi, Z. Gao, Y. Feng, G. Shen, X. Wang and D. Wang, High energy density, temperature stable lead-free ceramics by introducing high entropy perovskite oxide, *Chem. Eng. J.* **427**, 131684 (2022).

[22]F. Yan, X. Zhou, X. He, H. Bai and J. Zhai, Superior energy storage properties and excellent stability achieved in environment-friendly ferroelectrics via composition design strategy, *Nano Energy* **75**, 105012 (2020).

[23]Q. Xu, Z. Song, W. Tang, H. Hao, L. Zhang, M. Appiah, M. Cao, Z. Yao, Z. He and H. Liu, Ultra-wide temperature stable dielectrics based on $Bi_{0.5}Na_{0.5}TiO_3$-$NaNbO_3$ system, *J. Am. Ceram. Soc*. **98**, 3119 (2015).

[24]D. Han, C. Wang, X. Wei, P. Wang, Q. Liu, F. Meng, Z. Zeng and D. Wang, Ultrahigh energy efficiency of (1-x)$Ba_{0.85}Ca_{0.15}Zr_{0.1}$-$Ti_{0.9}O_3$-x$Bi(Mg_{0.5}Sn_{0.5})O_3$ lead-free ceramics, *J. Alloys Compd.* **902**, 163721 (2022).

[25]J. Sui, H. Fan, H. Peng, J. Ma, A. K. Yadav, W. Chao, M. Zhang and G. Dong, Enhanced energy-storage performance and temperature-stable dielectric properties of (1-x)[$(Na_{0.5}Bi_{0.5})0.95Ba_{0.05}$]0.98$La_{0.02}TiO_3$-x$K0.5Na_{0.5}NbO_3$ lead-free ceramics - ScienceDirect, *Ceram. Inter.* **45**, 20427 (2019).

[26]W. G. Ma, Y. W. Zhu, M. A. Marwat, P. Y. Fan, B. Xie, D. Salamon, Z. G. Ye and H. B. Zhang, Enhanced energy-storage performance with excellent stability under low electric fields in BNT-ST relaxor ferroelectric ceramics, *J. Mater. Chem. C* **7**, 281 (2019).

[27]E. Aksel, J. S. Forrester, B. Kowalski, M. Deluca and J. L. Jones, Structure and properties of Fe-modified $Na_{0.5}Bi_{0.5}TiO_3$ at ambient and elevated temperature, *Phys. Rev. B* **85**, 3125 (2012).

[28]T. Li, P. Chen, F. Li and C. Wang, Energy storage performance of $Na_{0.5}Bi_{0.5}TiO_3$-$SrTiO_3$ lead-free relaxors modified by $AgNb_{0.85}Ta_{0.15}O_3$, *Chem. Eng. J.* **406**, 127151 (2021).

[29]X. W. Jiang, H. Hao, Y. Yang, E. H. Zhou, S. J. Zhang, P. Wei, M. H. Cao, Z. H. Yao and H. X. Liu, Structure and enhanced dielectric

temperature stability of $BaTiO_3$-based ceramics by Ca ion B site-doping, *JMAT.* **7**, 295 (2021).

[30]Z. Chen, X. Bai, H. Wang, J. Du and Y. Zhang, Achieving high-energy storage performance in $0.67BiSmFeO_3$-$0.33BaTiO_3$ lead-free relaxor ferroelectric ceramics, *Ceram. Int.* **46**, 11549 (2020).

[31]B. Zhang, W. Wu, A. Khesro, P. Liu, M. Mao, K. Song, R. Sun and D. Wang, Outstanding discharge energy density and efficiency of the bilayer nanocomposite films with $BaTiO_3$-dispersed PVDF polymer and polyetherimide layer, *Chem. Eng. J.* **446**, 136926 (2022).

[32]H. Zhang, Q. Zhang, W. Ma, P. Fan, D. Salamon, S. T. Zhang, B. Nan, H. Tan and Z. G. Ye, A review on the development of lead-free ferroelectric energy-storage ceramics and multilayer capacitors, *J. Mater. Chem. C* **8**, 16648 (2020).

[33]Z. F. Li, B. Shen, H. R. Zeng, X. D. Jian and S. G. Lu, Multifunctionality of lead-free $BiFeO_3$-based ergodic relaxor ferroelectric ceramics: High energy storage performance and electrocaloric effect, *J. Alloy. Comp.* **803**, 185 (2019).